Current Opinion in Solid State and Materials Science 14 (2010) 107–115

Contents lists available at ScienceDirect

Current Opinion in Solid State and Materials Science

journal homepage: www.elsevier.com/locate/cossms

Piezo- and pyroelectric microscopy

Athanasios Batagiannis [a,*], Michael Wübbenhorst [b], Jürg Hulliger [a]

[a] Berne University, Department for Chemistry and Biochemistry, Freiestrasse 3, Bern, CH-3012, Switzerland
[b] Katholieke Universiteit Leuven, Laboratorium voor Akoestiek en Thermische Fysica, Celestijnenlaan 200D, B-3001, Leuven, Belgium

ARTICLE INFO

Article history:
Received 14 March 2010
Accepted 11 June 2010

Keywords:
Piezoelectric
Pyroelectric
Macroscopic polarization
Scanning probe microscopy

ABSTRACT

In recent decades piezo- and pyroelectricity found application in yet another important field of research. A number of methods have been developed which employ these properties to investigate the micro- and macroscopic polarization of materials. Advances in piezo- and pyroelectric imaging enabled researchers to examine the polarization distribution of a sample with unprecedented detail. This review attempts to inform the general reader about some of those experimental techniques and their findings.

1. Introduction

Piezoelectricity and pyroelectricity are manifestations of the dependence of spontaneous polarization on mechanical stress and temperature, respectively [1]. Piezoelectric and pyroelectric materials have a permanent, spontaneous polarization in the absence of an applied electric field. However, under constant stress and temperature, the polarization field is usually "masked" as nearby free charges are attracted to the surface of the sample thus creating a layer of bound charge that compensates the material's internal electric field originating from intrinsic dipoles. In order to measure a pyro- or piezoelectric effect a pressure or temperature perturbation is applied to the sample. The time-dependence of the excitation is usually distinguished into *harmonic* (periodical or continuous wave excitation) and *time-domain* excitations (pulse, step-excitations), giving rise to *dynamic* and *quasi-static* methods, respectively. In this review we will focus on *dynamic* methods, as they are most useful in determining a material's spatial polarization distribution. Table 1 summarizes some of those techniques and their characteristics.

The first demonstration of a dynamic method to measure the pyroelectric current was published by Chynoweth who applied it to study the pyroelectric effect and spontaneous polarization of barium titanate [2]. In essence, Chynoweth's technique demonstrated the physical basis which most subsequent thermal methods utilized. Let $\boldsymbol{P}_s$ be the spontaneous polarization per unit area of a face perpendicular to the polar axis, at a given temperature T. If the temperature is changed by a small increment dT (provided by a periodically modulated heat source) the polarization will also change by $d\boldsymbol{P}_s$. This change in polarization can be measured as a discharge current, $\boldsymbol{i}_p$, measured with a capacitor under short-circuit conditions [1]. The discharge current is

$$\boldsymbol{i}_p = \frac{dQ}{dt} = A\left(\frac{d\boldsymbol{D}}{dt}\right) = A\left(\frac{d\boldsymbol{P}_s}{dT}\right)\left(\frac{dT}{dt}\right) \quad (1)$$

where Q is the charge flowing through the external circuit, A is the electrode area, $\boldsymbol{D}$ is the electric displacement and dt the time increment over which temperature is changed. This equation holds provided that measurements are carried out under constant stress and electric field so as to avoid piezoelectric, ferroelastic and ferroelectric contributions. As all pyroelectric materials are also piezoelectric, the strain resulting from thermal expansion or contraction when temperature is changed induces a piezoelectric response. This is termed the secondary pyroelectric effect and it can be beneficial or antagonistic with the primary pyroelectric effect due to the polarization temperature dependence. However, it is generally small, typically not exceeding 10% of the magnitude of the primary effect. The rate of change of spontaneous polarization, $d\boldsymbol{P}_s/dT$, is the *pyroelectric coefficient*, $\boldsymbol{p}$, and for a small ΔT and sufficiently below the Curie temperature can be regarded as a constant for a given material and temperature. Hence, the pyroelectric current only depends on the rate of change of temperature and the pyroelectric coefficient is the proportionality constant between electric displacement and temperature.

It is precisely this behavior that allowed Chynoweth to show that the magnitude of the pyroelectric current is proportional to the net polarization of the sample measured. Furthermore, it was demonstrated that domains of opposite orientation produce currents of opposite sign. This important observation shows the value

* Corresponding author. Tel.: +41 031 631 4241; fax: +41 031 631 4244.
E-mail address: athanasios.batagiannis@gmail.com (A. Batagiannis).

1359-0286/$ - see front matter © 2010 Elsevier Ltd. All rights reserved.
doi:10.1016/j.cossms.2010.06.002

Table 1
Piezo- and pyroelectric microscopy techniques.

Method	References	Dimensionality	Resolution	Stimulus
Thermal pulse technique (TP)	[19–22, 68–70]	3D	1 μm	Thermal pulse
Laser intensity modulation method (LIMM)	[23–26, 55,56, 64–67]	3D	1 μm	Thermal wave
Scanning PyroElectric Microscopy (SPEM)	[77–80, 87–89]	3D	1 μm	Thermal wave
Light Induced Pressure Pulse method (LIPP)	[93–97]	1D	1 μm	Pressure pulse
Piezoelectric Pressure Step technique (PPS)	[98]	1D	1 μm	Pressure pulse
Pulsed electro-acoustic technique (EAT)	[99,100]	1D	1 μm	Voltage
Piezoresponse Force Microscopy (PFM)	[101–103]	3D	10 nm	Voltage
Scanning thermal microscopy (SThM)	[135]	3D	1 μm	Thermal wave

of the dynamic pyroelectric method in qualitative structure examination, as it provides information not accessible to standard X-ray diffraction. Measurements of the pyroelectric effect in barium titanate also demonstrated that a temperature change of 10^{-6} °C was enough to produce a measurable current and that the magnitude of this current was inversely proportional to the sample's thickness. Those findings led to the development of pyroelectric sensors in a wide range of applications [3–5].

Chynoweth's method was subsequently applied in the study of space charge [6], internal domains and pyroelectricity in ferroelectrics [7–9]. An interesting application employed additionally specific heat measurements [10] to study the ferroelectric–paraelectric transition in lithium tantalate. These early studies, however, were restricted to bulk measurements. An alternative method [11] employed a sharply focused electron beam as a heat source and electrostatic deflectors to scan the beam across the sample's area. Naturally, this method can provide higher resolution [12] than any of the photothermal methods. In the same period the first dynamic piezoelectric methods were being developed and applied to polarization switching studies in barium titanate [13,14].

Substantial improvements in instrumentation led to the development of the first scanning probe microscopes [15–17] capable of inspecting the polarization distribution in triglycine sulfate (TGS) and $BaTiO_3$ with resolution in the order of a few microns. These studies revealed how inhomogeneous the polarization distribution of crystals may be at a microscopic level and demonstrated the capabilities of the technique in identifying domain boundaries.

2. Techniques and applications

2.1. Photothermal methods

In the following years, thermal and pressure pulse techniques were used in a number of applications [18]. Two of the most widely used methods employed in the study of polarization distribution were the thermal pulse (TP) [19–22] technique developed by Collins and the light intensity modulation method (LIMM) [23–26] developed by Lang and Das-Gupta. The former was developed to study the pyroelectric current in the time domain and the latter in the frequency domain. Recent results demonstrated the equivalence of those approaches [27].

2.1.1. LIMM

A short description of LIMM is as follows: the sample under investigation is prepared as a thin sheet with its polar axis normal to the flat surfaces. Opaque electrodes are evaporated onto these surfaces. A sinusoidally modulated laser beam is focused on the electrode and heat diffuses into the sample as temperature waves. This results in a spatially non-uniform, time-varying temperature distribution, which, depending on the sample's polarization distribution, will produce a frequency dependent pyroelectric current. This current is amplified and measured at many different modulation frequencies. Although the technique is simple in its implementation, LIMM frequency response curves have to be deconvoluted using complex mathematical tools [28–36]. This is a result of unfavorable, diffusion-type attenuation profiles of thermal waves in the material. The expression relating the temperature increase and the pyroelectric coefficient with the pyroelectric current is a Fredholm integral [37] of the first kind and as such subject to the non-uniqueness problem. Another complication is the rapid decay of the spatial resolution with sample thickness [28], making it impossible to derive the polarization distribution away from the heated electrode. Furthermore, as with all measurement techniques the contribution from space charge to the pyroelectric response cannot be differentiated from the polarization contribution.

Despite those disadvantages and the experimental difficulties [38], LIMM has proved to be extremely useful in a wide range of applications. It has been used to study the polarization distribution in ceramics [39–43], polymers [34,44–55], single crystals [56–59] and liquid crystals [60–63]. Because of the aforementioned problems, in most cases the technique has been applied to the study of bulky materials but the lateral resolution was limited. In order to overcome the difficulties in determining the polarization distribution near a sample's surface Lang and collaborators have extended the LIMM to higher frequencies calling it the surface light intensity modulation method (SLIMM) [55,56,64]. The extent of propagation of heat in the sample is governed by the thermal diffusion depth, given by:

$$\mu = \sqrt{2\alpha/\omega} \tag{2}$$

where ω is the modulation angular frequency and α the material's thermal diffusivity. It is clear from the above equation that increasing the modulation frequency limits the penetration of the thermal wave inside the sample. The smaller the volume of the thermally excited area is, the higher the resolution that can be achieved.

Another drawback in the application of LIMM is the large diameter of the laser spot when compared to the sample's thickness. This is done to reduce the problem of spectra deconvolution using a simpler 1D approach. However, recently a number of applications have emerged [65–76] where the laser beam is focused and used as a scanning probe. A recent example of such a study is shown in Fig. 1. The authors used LIMM to investigate defects and depoling caused by mechanical and thermal treatments in lead zirconate titanate (PZT) ceramic materials [71]. Fig. 1 demonstrates the pyroelectric activity exhibited by a soft PZT sample after exposure to a high-power micromachining laser. The areas exposed show a decreased pyroelectric activity (depicted in blue) when compared with unexposed areas on the sample (depicted in red). Additional experiments using a solder tip or compressive stress along the poling direction yielded similar results, thus demonstrating the value of the technique in material characterization.

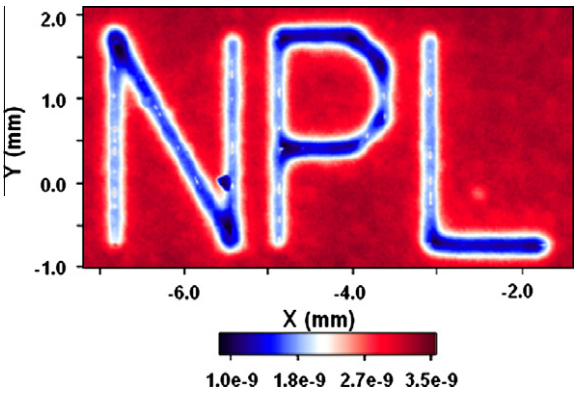

Fig. 1. LIMM image of a PZT sample after exposure to a high-power Nd-YAG laser. Modified after Ref. [71].

2.1.2. TP

The slow data acquisition speed has prompted researchers to invent new methods in order to investigate the polarization distribution using scanning probe microscopies. The thermal pulse (TP) technique [19–22,68–70] has proved to be the most efficient as it can achieve data acquisition speeds 50 times faster that those of LIMM. A recent study [68] has shown that results obtained from the same sample using both methods are in excellent agreement. In TP samples are also prepared as a thin film which is coated with aluminum or copper electrodes to form a capacitor. The heat source, however, is usually a pulsed laser beam which is focused onto an opaque electrode. The thermal pulses generated, diffuse into the material which causes a pyroelectric response. The resulting current is then amplified and recorded using a lock-in technique or a digital oscilloscope. The high speed and resolution, as well as the applicability in relatively thick samples are the main advantages of this method.

Mellinger et al. [70] have employed TP to study space charge and polarization distributions in electret polymers. Their results showed that lateral resolutions of 50 μm can be achieved with a depth resolution of 0.5 μm. Fig. 2 shows the polarization map of a piezoelectric PVDF-TrFE co-polymer sensor cable. The authors removed the cable's core and replaced it with a stainless steel pin which they used to pole the cable. The blue crosses in the figure indicate the pin's position. Measurements were taken at various modulation frequencies thus achieving various depths of thermal excitation indicated on the *z*-axis. The samples show a smooth polarization distribution centered on the needle's position. This is in sharp contrast with results from commercial sensor cables that show an inhomogeneous polarization distribution [70].

2.1.3. SPEM

LIMM and TP techniques are especially suited to study the polarization distribution in thin films but they cannot be used as effectively to investigate bulky 3D objects such as crystals. In order to tackle this problem, Wübbenhorst et al. have devised an alternative methodology [38,77–89]. Instead of illuminating the front electrode they focused the beam directly onto the sample's surface. This requires a greater distance between the electrodes which makes measurement of small signals harder, however, much higher resolutions (<10 μm) can be achieved.

In SPEM samples are placed in a capacitor and heated using a laser beam modulated by an acousto-optic modulator or an optical chopper. The beam is focused with a resolution of a few microns on a pyroelectric material and scanned throughout the sample's surface. The signal is amplified with a current amplifier and measured with a lock-in amplifier, which also provides the reference modulation frequency. Plotting the successive measurements of the resulting pyroelectric current on a 2D contour plot allows one to visualize the spatial distribution of the macroscopic polarization of the sample. As in the case of LIMM, measuring or estimating the material's thermal diffusivity allows one to choose the exact depth within the sample to be stimulated. The drawback is that the measurements are taken at a single modulation frequency and thus the data represent polarization distributions at a specific depth within the sample. The technique could be modified, however, to facilitate simultaneous frequency as well as position scanning.

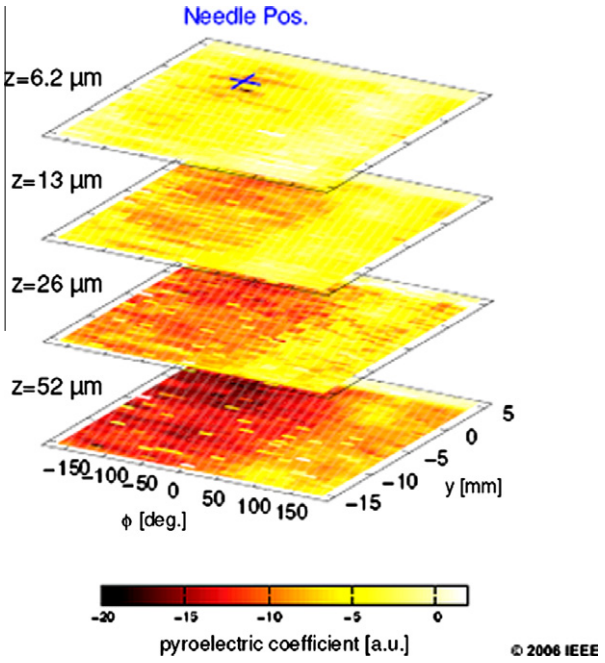

Fig. 2. Spatial polarization map of a PVDF-TrFE copolymer sensor cable [70].

Scanning PyroElectric Microscopy (SPEM) was initially applied to the study of polarization distributions in chromophore–zeolite composites [77,78]. In those systems, a guest chromophore molecule is included in the parallel channels of a zeolite. There were two models attempting to explain the ordering of guest molecules in molecular sieves: (i) the guest–host interaction gives rise to acentric molecular arrangements [90] or (ii) the adsorption of the guest molecule into the channels takes place in a preferred orientation thus leading to a bipolar arrangement [91]. According to (i) the crystal would show the same sign throughout its length for the pyroelectric current whereas if (ii) was true the current should switch signs at some point along the channel axis. Using SPEM the authors were able to show that the latter holds although subsequent investigations [83] revealed that the zeolite crystals were also twinned, i.e. they are macroscopically symmetric and show two opposite macrodomains.

A further development came from Quintel et al. who used tomographic methods to study the polarization distribution in perhydrotriphenylene (PHTP) co-crystallized with 1-(4-nitrophenyl)-piperazine (NPP) [87]. Theoretical predictions [82,92] and previous SPEM measurements had revealed the double-cone structure of the polarization distribution for channel-type inclusion compounds. The authors measured the pyroelectric image, then successively polished the crystal in four steps and repeated the measurement after each step. The results can be seen in Fig. 3, showing two main cone-shaped areas of opposite polarity depicted with red for positive and blue for negative current respectively. It is also clear that the outer domains along the *x*-axis are less polarized. In the center

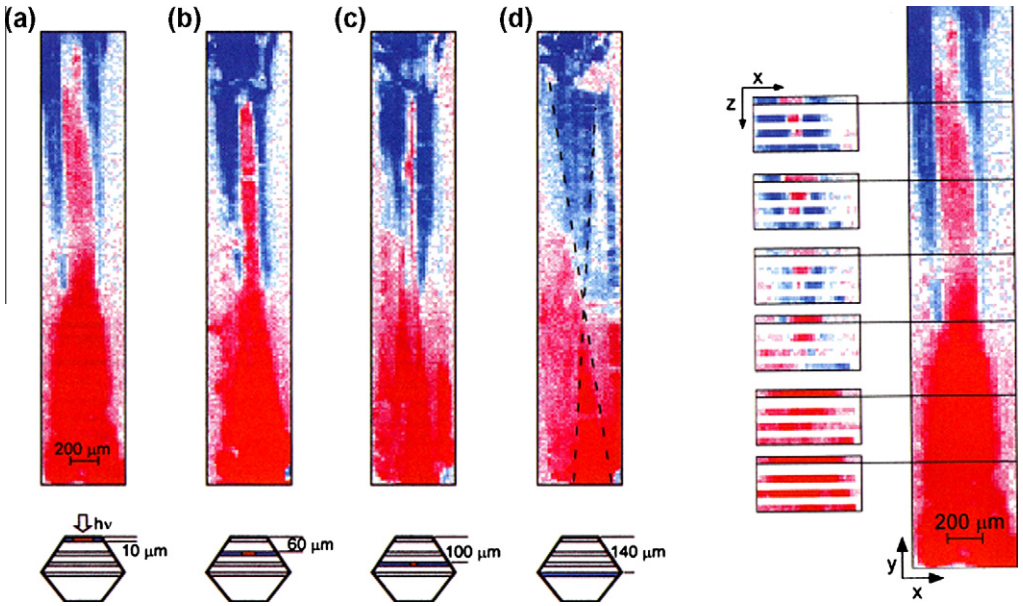

Fig. 3. SPEM images of a PHTP-NPP single crystal successively polished in four steps (a–d). The composite image on the far right gives a tomographic view of those images [87].

we observe a white area signifying the diminishing of pyroelectric activity. This is attributed to the location of the seed. The composite image on the far right shows the pyroelectric distribution as a function of depth for selected areas. It is easily observed that the structure changes as we progress into the sample with a nearly perfect hourglass-like form near the middle of the crystal (Fig. 3d). Based on those observations the authors concluded that PHTP-NPP nucleates creating a non-polar seed which is then subjected to a growth mechanism that results in a bipolar, hourglass-shaped polarization distribution.

A more recent SPEM study was undertaken to investigate the polarization distribution in 4-bromo-4′-biphenyl. Pyramid-shaped crystals showed a strong second harmonic generation effect and they were subsequently analyzed using SPEM. Fig. 4 shows the peculiar domain structure of 4-bromo-4′-biphenyl as revealed by lateral pyroelectric scanning. Two domains of opposite polarity are clearly visible with the strength of the pyroelectric current varying as indicated by the colour bar next to the graph. The domains are inter-twinned and they correspond well to the topography of the crystal. X-ray analysis has shown that the crystallographic *b*-axis lies in the direction out of the plane (Labat G, Bonin M, Couderc G, Batagiannis A, Berger R, Buergener M, Merz K, Wübbenhorst M, Hulliger J, unpublished data).

2.2. Pressure pulse methods

2.2.1. LIPP

Another approach in the study of polarization distributions is to stimulate the sample using a pressure pulse resulting in a piezoelectric response from the sample. The most common technique

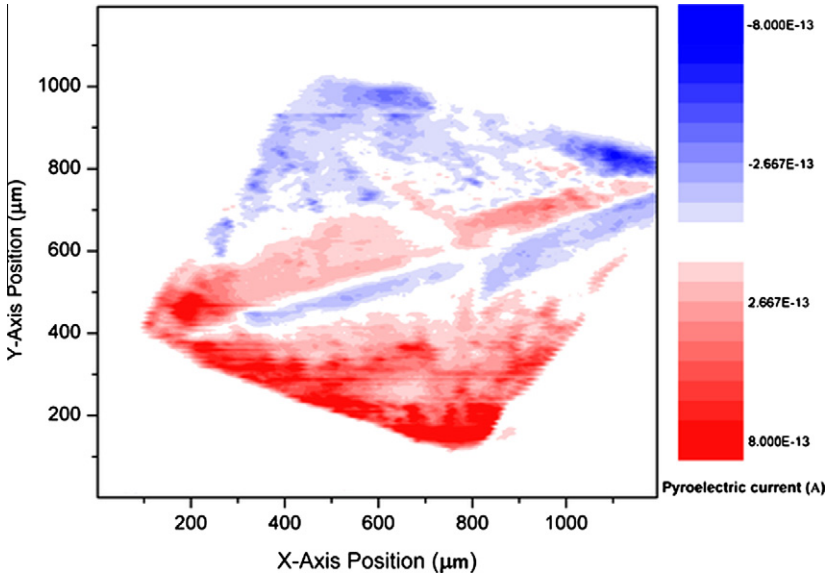

Fig. 4. SPEM measurement of a twinned 4-bromo-4′-biphenyl crystal.

employed is the Light Induced Pressure Pulse method (LIPP) [93–95]. A high-energy laser is focused on the front electrode where it is absorbed. The short laser pulses thus cause mechanical stress, which in turn results in the generation of a pressure pulse that propagates into the sample. This pulse travels through the sample with the velocity of sound and is reflected at the rear surface. The resulting piezoelectric current is amplified and recorded using a digital oscilloscope. Ideally, the spatial charge distribution is directly proportional to the measured current response. An alternative configuration uses a piezoelectric transducer to generate the pressure pulse [96,97]. LIPP results have been shown to be in good agreement with LIMM measurements [51], however, it too suffers from limited knowledge of the actual pressure wave propagation within a sample.

2.2.2. PPS

The Piezoelectric Pressure Step (PPS) [98] technique is another acoustic method providing essentially the same information. This method is very similar to LIPP, relying on a propagating pressure wave to induce a piezoelectric response from the sample. The main modification is that the pressure wave generated by the laser beam is recorded by a quartz crystal bonded on the back side of the sample. The resolution of this method depends on the width of the pressure wave. In order to satisfy the conditions required for the measured current to be a unique solution of the polarization distribution strict mechanical prerequisites must be met. If the pulse is sufficiently short (<1 ns), the electrical response gives the spatial distribution of the electric field and charge density. The main advantages of this method are its applicability to surface charge measurements and thick samples (up to 200 μm).

2.2.3. PEA

The pulsed electro-acoustic (PEA) [99,100] technique, has been developed to enable simultaneous measurement of the space charge and electric field distributions as a function of temperature within a sample. The method relies on the application of a voltage pulse across the sample to provide stimulation. The induced electric field exerts a force on individual charges at charge layers near the electrodes. Thus, acoustic waves are generated as a result of momentum exchange between the electrical charges and the medium. The wave's amplitude is proportional to the local charge density. The technique employs a piezoelectric transducer to detect those waves. An external heater allows the sample to be heated to temperatures up to 90 °C. The resolution of this method depends on the duration of the electric pulse and on the thickness of the sample. The polarization and space charge density profiles are obtained from a Fourier transform procedure.

2.3. Techniques based on scanning probe microscopy

2.3.1. PFM

In recent years numerous attempts have been made to push the limits of resolution to the nanometer scale. The most successful of those attempts led to the development of Piezoresponse Force Microscopy (PFM) [101–103]. In PFM the tip of an Atomic Force Microscope (AFM) is used to apply an Alternating Current (AC) voltage onto the sample. The tip is in contact with the sample and hence the bias-induced reverse piezoelectric response causes a deformation of the sample's surface. This in turn results in the deflection of the tip which is measured by monitoring the cantilever's position. The first harmonic of the signal is proportional to the polarization distribution and under certain conditions the

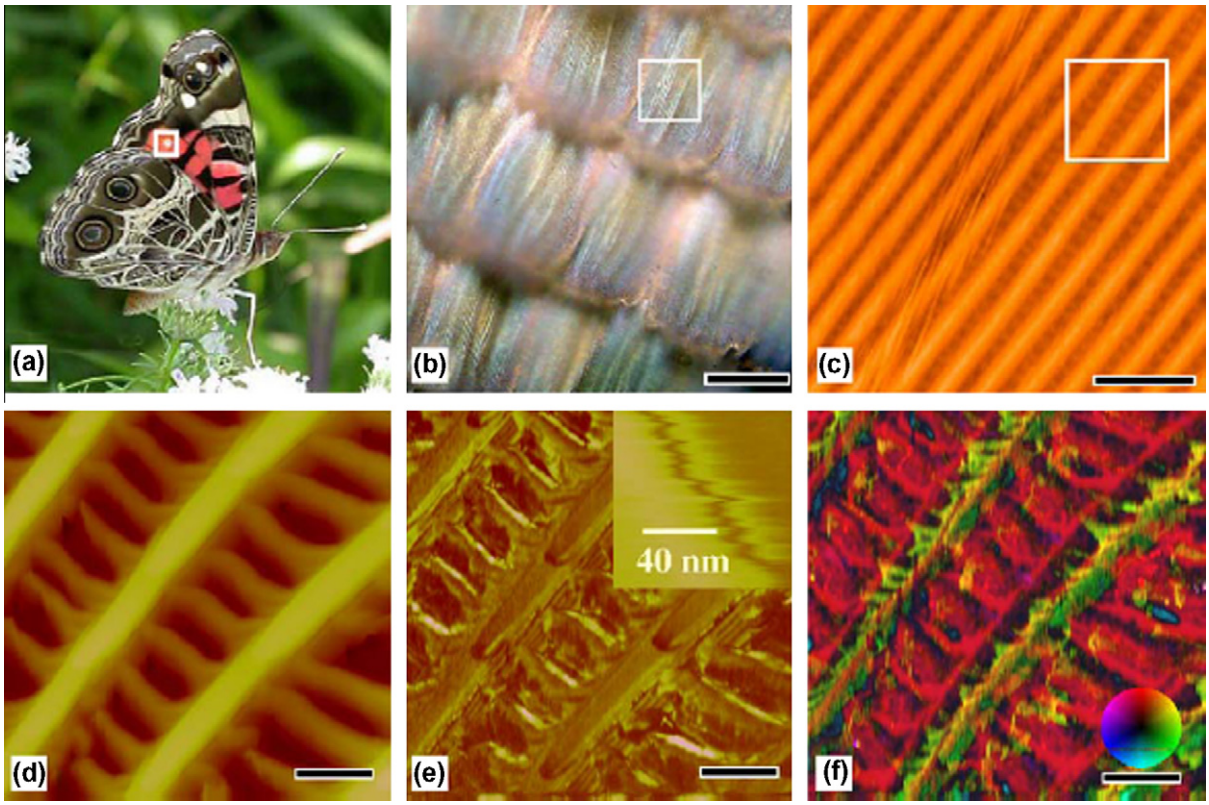

Fig. 5. (a) Photograph of *Vanessa Virginiensis*. (b) Optical close-up of the area studied. (c and d) AFM surface topography of the area studied. (e) Elasticity image of the same area. (f) Vector PFM image showing the piezoresponse from the butterfly's wing. The signal's contrast reveals the complex array orientation of chitin molecules. The scale is 50 (b), 5 (c) and 1 μm (d–f), respectively [131].

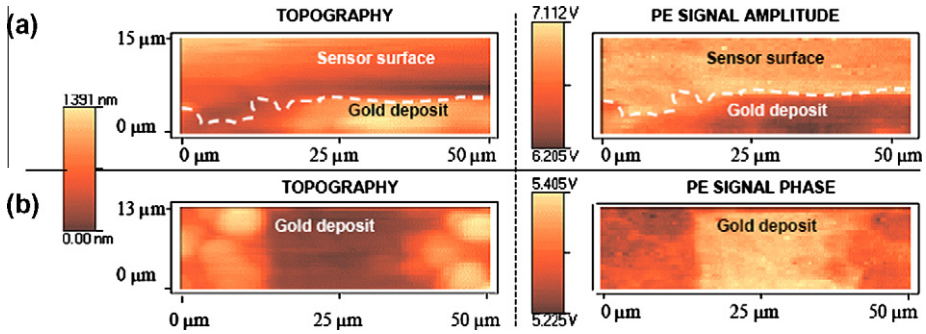

Fig. 6. (a) SThM-PE Amplitude and (b) phase compared to the sample's topography on the left side of a $LiTaO_3$ crystal [135].

piezoelectric coefficient can be determined. The phase of the response contains information about the local direction of polarization in the area directly below the tip. The resolution of the technique is in the order of a few nanometers.

The method was initially developed to study ferroelectric materials [104–111] at the nanoscale. It has enabled imaging of ferroelectric grains, domains, boundaries and dynamic processes with unprecedented detail. In a recent development, researchers were able to show using PFM that in certain ferroelectric materials [112,113], the direction of polarization switches along the polar axis, contrary to the established belief, i.e. that the polarization direction of the crystal seed during crystallization determines the absolute polar axis. Further details on PFM and its findings can be found in recent reviews [114–118] where the physical mechanism, experimental details and practical applications of PFM are discussed at length.

The above successes of PFM led to its adaptation by the scientific community to study amongst others the manipulation and characterization of crystals [119], polymers [120,121], multiferroics [122], Langmuir–Blodgett films [123], nanoparticles [124], and nanotubes [125]. More interestingly perhaps, recently researchers are turning their attention to the polarization distribution of some biological materials known to be polar [126,127]. The polarity of biologic materials is of course a result of acentric packing of polar proteins such as chitin, collagen and keratin. A number of studies [128–133] were published that map the polarization distribution of these proteins in biological tissue.

Fig. 5 shows an example of such a study. PFM was used to map the polarization distribution on the wings of butterfly *Vanessa Virginiensis* (American Lady) [131]. The wing of the butterfly is covered by chitin scales where chitin rods are embedded in a protein matrix (a–d). The vector PFM map (f) reveals inhomogeneous piezoelectric properties. The authors ascribed those properties to a complex organization of chitin chains since the piezoresponse does not diminish to zero perpendicular to the molecular axis. Hence in this case we do not observe a simple unipolar arrangement as reported for collagen type I [133].

2.3.2. SThM

Similarly impressive resolutions have been recently achieved using another variation of the AFM. Other photothermal imaging techniques have developed in parallel with piezo- and pyroelectric microscopy and many times their methods and results are complementary (for a review of thermal techniques see Pollock and Hammiche [134]). Scanning thermal microscopy (SThM) is such a technique. The sample is placed on a pyroelectric sensor and heated locally with a heat probe. From the pyroelectric signal, useful information can be extracted such as the thermal conductivity and the thermal diffusivity of the material. Although the technique cannot provide polarization distribution measurements, it is mentioned here since the data gathered are complementary to pyroelectric methods.

Antoniow et al. have replaced the tip of the AFM with a micromachined Wollaston wire [135] thus acting as a local modulated heat source. They used it to study the thermal properties of a gold layer deposited on a $LiTaO_3$ ferroelectric crystal. The results are shown in Fig. 6. The pyroelectric response in (a) is in good agreement with topography and shows many details. The additional heat capacity of the gold film results in a decrease in the pyroelectric signal as expected.

3. Conclusions and outlook

Piezo- and pyroelectric techniques have developed significantly in the last few years and they can now be used to map the polarization distribution in one, two or three dimensions, down to sub-µm resolution. PFM in particular has demonstrated the resolution of nano-sized polar structures [119–125]. Its findings have already provided useful information about polarity in materials and biological tissue [128–133]. The resolution of the pyroelectric techniques may be further improved using a modified AFM like the one employed by Antoniow et al. [135] allowing for electrodes to be placed perpendicular to the sample's polar axis. Furthermore, the combination of his technique with pyroelectric characterization might give precise thermal profiling and thus improve the uncertainty in the determination of the polarization distribution. Alternatively, Burfoot and Latham's [11] electron beam technique could be modernized in order to achieve ultrahigh resolutions. In the study of the polarization distribution in biomaterials and nanostructures such resolutions are required to investigate one of nature's greatest secrets; the spontaneous formation of polar nanostructures and their physiological significance in organisms [126,127].

References

[*] *Recommended.*
[**] *Highly recommended.*

[1] Lang SB. Sourcebook of pyroelectricity. New York: Gordon and Breach; 1974.
[2] Chynoweth AG. Dynamic method for measuring the pyroelectric effect with reference to barium titanate. J Appl Phys 1956;27:78–84.
[3] Hadni A, Henninger Y, Thomas R, Vergnat P, Wyncke B. Sur les propriétés pyroélectriques de quelques matériaux et leur application à la détection de l'infrarouge. J Phys 1965;26:345–60.
[4] Hadni A. Applications of the pyroelectric effect. J Phys E Sci Instrum 1981;14:1233–40.
[*5] Lang SB, Muensit S. Review of some lesser-known applications of piezoelectric and pyroelectric polymers. Appl Phys A 2006;85:125–34. Reviews many applications of piezoelectric and pyroelectric polymers and outlines their advantages and disadvantages when compared with other materials.
[6] Chynoweth AG. Surface space-charge layers in barium titanate. Phys Rev 1956;102:705–14.

[7] Chynoweth AG. The pyroelectric behaviour of colemanite. Acta Crystallogr 1957;10:511–4.

[8] Perls TA, Diesel TJ, Dobrov WI. Primary pyroelectricity in barium titanate ceramics. J Appl Phys 1958;29:1297–302.

[9] Glass AM. Investigation of the electrical properties of $Sr_{1-X}Ba_XNb_2O_6$ with special reference to pyroelectric detection. J Appl Phys 1969;40: 4699–713.

[10] Glass AM. Dielectric, thermal, and pyroelectric properties of ferroelectric $LiTaO_3$. Phys Rev 1968;172:564–71.

[**11] Burfoot JC, Latham RV. A new method for studying movements of electric domain walls. Brit J Appl Phys 1963;14:933–4. Demonstrates the feasibility of using an electron beam to induce a pyroresponse from a polar material and thus study its polarization distribution. Also shows detection of movements of electric domain walls. Modernization of the technique could lead to ultra high resolution mapping of the polarization distribution.

[12] Hadni A. Comparison of the laser scanning microscopy for pyroelectric display in real time, with other methods to study domains structure, a review. Ferroelectrics 1993;140:25–32.

[13] Husimi K, Kataoka K. Ultrasonic measurement of polarization switching processes in barium titanate single crystal. J Appl Phys 1958;29:1247–51.

[14] Husimi K, Kataoka K. Nondestructive measuring method of polarization for the study of ferroelectrics. Rev Sci Instrum 1960;31:418–21.

[15] Clay W, Evans BJ, Latham RV. A nondestructive pyroelectric display of an antiparallel polarization distribution in single-crystal barium titanate. J Phys D Appl Phys 1974;7:1291–5.

[16] Hadni A, Bassia JM, Gerbaux X, Thomas R. Laser scanning microscope for pyroelectric display in real time. Appl Optics 1976;15:2150–8.

[17] Hadni A, Thomas R. Laser study of reversible nucleation sites in triglycine sulphate and applications to pyroelectric detectors. Ferroelectrics 1972;4:39–51.

[18] Busse G. Imaging with optically generated thermal waves. IEEE Trans Son Ultrason 1985;32:355–64.

[19] Collins RE. Analysis of spatial distribution of charges and dipoles in electrets by a transient heating technique. J Appl Phys 1976;47:4804–8.

[20] Collins RE. Measurement of charge distribution in electrets. Rev Sci Instrum 1977;48:83–91.

[21] Collins RE. Practical application of the thermal pulsing technique to the study of electrets. J Appl Phys 1980;51:2973–86.

[22] Collins RE. The thermal pulsing technique applied to polymer electrets. Ferroelectrics 1981;33:65–74.

[23] Lang SB, Das-Gupta DK. A technique for determining the polarization distribution in thin polymer electrets using periodic heating. Ferroelectrics 1981;39:1249–52.

[24] Lang SB, Das-Gupta DK. Complex polarization distributions in PVDF samples. Ferroelectrics 1984;55:151.

[25] Lang SB, Das-Gupta DK. A new technique for determination of the spatial distribution of polarization in polymer electrets. Ferroelectrics 1984;60:23–36.

[26] Lang SB, Das-Gupta DK. Laser-intensity-modulation method: a technique for determination of spatial distributions of polarization and space charge in polymer electrets. J Appl Phys 1986;59:2151–60.

[**27] Mellinger A, Flores-Suárez R, Singh R, Wegener M, Wirges W, Gerhard-Multhaupt R, et al. Thermal-pulse tomography of space-charge and polarization distributions in electret polymers. Int J Thermophys 2008;29:2046–54. Describes a novel, improved technique to study the 3D polarization distribution of polarization in polar materials. The technique is much faster than LIMM and its resolution is not limited by deconvolution constraints.

[28] von Seggern H. Thermal-pulse technique for determining charge distributions: effect of measurement accuracy. Appl Phys Lett 1978;33: 134–7.

[29] Lang SB. Laser intensity modulation method (LIMM): experimental techniques, theory and solution of the integral equation. Ferroelectrics 1991;118:343–61.

[30] Lang SB. An analysis of the integral equation of the surface laser intensity modulation method using the constrained regularization method. IEEE Trans Dielectr Electr Insul 1998;5:70–6.

[**31] Lang SB. Laser intensity modulation method (LIMM): review of the fundamentals and a new method for data analysis. IEEE Trans Dielectr Electr Insul 2004;11:3–12. A comprehensive review of the LIMM method with particular emphasis on the deconvolution problem. Simulated and experimental data are analyzed with a new technique that gives the polarization distribution in the form of a special 8th-degree polynomial.

[32] Lang SB. Fredholm integral equation of the laser intensity modulation method (LIMM): solution with the polynomial regularization and L-curve methods. J Mater Sci 2006;41:147–53.

[33] Ploss B, Emmerich R, Bauer S. Thermal wave probing of pyroelectric distributions in the surface region of ferroelectric materials: a new method for the analysis. J Appl Phys 1992;72:5363–70.

[34] Bloss P, Schäfer H. Investigations of polarization profiles in multilayer systems by using the laser intensity modulation method. Rev Sci Instrum 1994;65:1541–50.

[35] Mellinger A. Unbiased iterative reconstruction of polarization and space-charge profiles from thermal-wave experiments. Meas Sci Technol 2004;15:1347–53.

[36] Bauer S, Bauer-Gogonea S. Current practice in space charge and polarization profile measurements using thermal techniques. IEEE Trans Dielectr Electr Insul 2003;10:883–902.

[37] Prössdorf S, Silbermann B. Numerical analysis for integral and related operator equations – operator theory advances and applications. Basel: Birkhauser; 1991.

[38] Wübbenhorst M, van. Turnhout J. Thermal wave methods: some experimental pitfalls. In: IEEE 8th intern sympos electrets, Paris; 1994. p. 182–7.

[39] Lang SB, Yin QR. Spatial distributions of polarization and space charge in tin-substituted lead zirconate titanate ceramics using laser intensity modulation method (LIMM). Ferroelectrics 1987;74:357–68.

[40] Cheng Z, Yao X. Space charge distribution measurement of PLZT ceramics. Ferroelectrics 1990;109:155–60.

[41] Boue C, Alquie C, Fournier D. High spatial resolution of permanent polarization distributions in ferroelectric samples using a combination of PWP and LIMM measurements. Ferroelectrics 1997;193:175–88.

[42] Lang SB, Li G. Rainbow ceramics: processing techniques; piezoelectric, dielectric and pyroelectric properties; and polarization distributions as determined with SLIMM. J Korean Phys Soc 1998;32:S1268–71.

[43] Suchaneck G, Koehler R, Sandner T, Gerlach G, Deineka A, Jastrabik L, et al. Polarization profile of RF-sputtered self-polarized PZT thin films. Integr Ferroelectr 2001;32:861–9.

[44] Wübbenhorst M, Petzsche T, Ruscher C. Determination of the spatial polarization distribution in poly(vinylidene fluoride) films by the laser intensity modulation method. Ferroelectrics 1988;81:1337–40.

[45] Wübbenhorst M, Petzsche T. Messung der räumlichen polarisationsverteilung in poly-(vinylidenfluorid) mittels der laser-intensitäts-modulations-methode. Acta Polym 1988;39:201–6.

[46] Thiele V, Wübbenhorst M. The application of the laser intensity modulation method (LIMM) for the study of the poling behavior of polyamide 11. Acta Polym 1992;43:61–2.

[47] Das-Gupta DK, Hornsby JS. A non-destructive technique for the determination of spatial charge and polarization distributions in insulating polymers. J Phys D Appl Phys 1990;23:1485–90.

[48] Wübbenhorst M, Wünsche P. Inhomogeneous distributions of polarization in polyvinylidene fluoride mono- and multilayer films studied by the laser intensity modulation method. Prog Coll Pol Sci 1991;85:23–37.

[49] Bauer S, Ploss B. Polarization distribution of thermally poled PVDF films, measured with a heat wave method (LIMM). Ferroelectrics 1991;118:363–78.

[50] Yilmaz S, Bauer S, Wirges W, Gerhard-Multhaupt R. Scanning electro-optical and pyroelectrical microscopy for the investigation of polarization patterns in poled polymers. Appl Phys Lett 1993;63:1724–6.

[51] Das-Gupta DK, Hornsby JS, Yang GM, Sessler GM. Comparison of charge distributions in FEP measured with thermal wave and pressure pulse techniques. J Phys D Appl Phys 1996;29:3113–6.

[52] Bloss P, Steffen M, Schafer H, Eberle G, Eisenmenger W. Polarization and electric field distribution in thermally poled PVDF and FEP. IEEE Trans Dielectr Electr Insul 1996;3:417–24.

[53] Bloss P, Steffen M, Schafer H, Guo Mao Y, Sessler GM. Determination of the polarization distribution in electron-beam-poled PVDF using heat wave and pressure pulse techniques. IEEE Trans Dielectr Electr Insul 1996;3:182–90.

[54] Bloss P, Steffen M, Schafer H, Yang GM, Sessler GM. A comparison of space-charge distributions in electron-beam irradiated FEP obtained by using heat-wave and pressure-pulse techniques. J Phys D Appl Phys 1997;30: 1668–75.

[55] Lang SB. Determination of the polarization distribution in a weakly-poled PVDF film using the surface laser intensity modulation method (SLIMM). Mater Chem Phys 2003;79:154–6.

[56] Lang SB, Kugel VD, Rosenman G. Direct observation of domain inversion in heat-treated $LiNbO_3$ using surface laser intensity modulation method (SLIMM). Ferroelectrics 1994;157:69–74.

[57] Lang SB, Rosenman G, Rushin S, Kugel V, Nir D. Electron emission and spontaneous polarization distribution of proton-exchanged $LiNbO_3$. Ferroelectrics 1992;133:253–8.

[58] Krug R, Würfel P, Ruppel W. Material characterization with a simple laser scanning microscope. Appl Optics 1993;15:6458–63.

[**59] Movchikova AA, Suchaneck G, Malyshkina OV, Gerlach G. Characterization of ferroelectrics by thermal wave methods. J Eur Ceram Soc 2007;27:4007–10. Spatial profiles of the polarization distribution of SBN crystals, $BaTi_{1-x}Sn_xO3$ ceramics, and $Pb(Zr,Ti)O_3$ thin films are determined from pyroelectric current measurements. Describes a new solution of the Fredholm integral equation by a Tikhonov regularization method.

[60] Steffen M, Bloss P, Schafer H, Winkler M, Geschke D. Investigations of polarization profiles in sandwich cells containing a liquid crystalline polymer by using the heat wave method (LIMM). Liq Cryst 1995;19:93–7.

[61] Leister N, Geschke D. Pyroelectric investigations of polarization and charge distributions in sandwich cells containing a ferroelectric liquid crystalline polymer. Liq Cryst 1998;24:441–9.

[62] Lehmann W, Leister N, Hartmann L, Geschke D, Kremer F, Stein P, et al. Piezoelectric and pyroelectric investigations on microtomized sections of single-crystalline ferroelectric liquid crystalline elastomers (SC-FLCE). Mol Cryst Liq Cryst 1999;328:437–45.

[63] Feller F, Geschke D, Kozlovsky MV. Ferroelectric polarization hysteresis in a liquid crystal polymer by means of LIMM. Mol Cryst Liq Cryst 2001;357:167–75.

[64] Lang SB, Jiang Q. Ion-beam etched PLZT samples and analysis by means of the surface laser intensity modulation method (SLIMM). Ferroelectrics 1996;186:53–6.
[65] Marty-Dessus D, Berquez L, Petre A, Franceschi JL. Space charge cartography by FLIMM: a three-dimensional approach. J Phys D Appl Phys 2002;35:3249–56.
[66] Petre A, Marty-Dessus D, Berquez L, Franceschi JL. A comparison of different mathematical treatments for solving the inverse problem in focused laser intensity modulation method. Jpn J Appl Phys 2004;43:2574–9.
[*67] Petre A, Marty-Dessus D, Berquez L, Franceschi JL. Space charge cartography by FLIMM on SEM-irradiated PTFE thin films. J Electrostat 2006;64:492–7. Presents the results obtained by focused laser-intensity modulation method (FLIMM) on polytetrafluoroethylene (PTFE) thin films irradiated by electron beam. Shows how laser surface scanning allows retrieving the charge boxes and determining their implanted depth. Demonstrates lateral resolution of 10 μm. The space charge evolution with time is presented and gives an indication of their migration inside the structure.
[68] Mellinger A, Singh R, Gerhard-Multhaupt R. Fast thermal-pulse measurements of space-charge distributions in electret polymers. Rev Sci Instrum 2005;76:013903.
[69] Mellinger A, Singh R, Wegener M, Wirges W, Gerhard-Multhaupt R, Lang SB, et al. Appl Phys Lett 2005;86:082903.
[**70] Mellinger A, Flores-Suárez R, Wegener M, Wirges W, Gerhard-Multhaupt R, Singh R. Thermal-pulse tomography of polarization distributions in a cylindrical geometry. IEEE Trans Dielectr Electr Insul 2006;13:1030–5. Demonstrates fast, three-dimensional polarization mapping in piezoelectric sensor cables by thermal-pulse tomography (TPT) technique with a lateral resolution of 200 μm.
[*71] Stewart M, Cain M. Spatial characterization of piezoelectric materials using the scanning laser intensity modulation method (LIMM). J Am Ceram Soc 2008;91:2176–81. Shows the capability of LIMM to detect various types of defects in PZT ceramic materials including localized sample depoling brought about through thermal and mechanical treatments. It also demonstrates detection of defects due to environmental degradation under high dc bias.
[72] Donval A, Berkovic G, Yilmaz S, Bauer-Gogonea S, Brinker W, Wirges W, et al. Spatial and thermal analysis of optical nonlinearity created by asymmetric charge injection. Optics Commun 1996;123:195–200.
[73] Das-Gupta DK, Tunnicliffe D. In: IEEE 10th intern sympos electrets, Athens; 1999. p. 569–72.
[74] Bune AV, Zhu C, Ducharme S, Blinov LM, Fridkin VM, Palto SP, et al. Piezoelectric and pyroelectric properties of ferroelectric Langmuir–Blodgett polymer films. J Appl Phys 1999;85:7869–73.
[75] Shtykov NM, Vij JK. Measurement of the polarization profile across a surface-stabilized ferroelectric liquid crystal cell using the pyroelectric laser-intensity-modulation method. J Appl Phys 2003;93:159–64.
[76] Peterson BW, Ducharme S, Fridkin VM, Reece TJ. Mapping surface polarization in thin films of the ferroelectric polymer P(VDF-TrFE). Ferroelectrics 2004;304:51–4.
[77] Caro J, Marlow F, Wübbenhorst M. Chromophore–zeolite composites: the organizing role of molecular sieves. Adv Mater 1994;6:413–6.
[78] Marlow F, Wübbenhorst M, Caro J. Pyroelectric effects on molecular sieve crystals loaded with dipole molecules. J Phys Chem 1994;98:12315–9.
[79] Hulliger J, Rogin P, Quintel A, Rechsteiner P, König O, Wübbenhorst M. The crystallization of polar, channel-type inclusion compounds: property-directed supramolecular synthesis. Adv Mater 1997;9:677–80.
[80] Quintel A, Hulliger J, Wübbenhorst M. Analysis of the polarization distribution in a polar perhydrotriphenylene inclusion compound by scanning pyroelectric microscopy. J Phys Chem B 1998;102:4277–83.
[81] Klap GJ, van Klooster SM, Wübbenhorst M, Jansen JC, van Bekkum H, van Turnhout J. Polarization reversal in $AlPO_{4-5}$ crystals containing polar or nonpolar organic molecules: a scanning pyroelectric microscopy (SPEM) study. J Phys Chem B 1998;102:9518–24.
[82] Roth SW, Langley PJ, Quintel A, Wübbenhorst M, Rechsteiner P, Rogin P, et al. Statistically controlled self-assembly of polar molecular crystals. Adv Mater 1998;10:1543–6.
[83] Klap GJ, Wübbenhorst M, Jansen JC, van Koningsveld H, van Bekkum H, van Turnhout J. Polar growth and directional adsorption of large $AlPO_{4-5}$ crystals determined by scanning pyroelectric microscopy. Chem Mater 1999;11:3497–503.
[84] Müller T, Hulliger J, Seichter W, Weber E, Weber T, Wübbenhorst M. A new organic nanoporous architecture: dumb-bell-shaped molecules with guests in parallel channels. Chem Eur J 2000;6:54–61.
[85] Wübbenhorst M, van Turnhout J, Quintel A, Hulliger J. Spatially resolved heat conduction in polar perhydrotriphenylene inclusion compounds studied by means of thermal waves. J Appl Phys 2000;88:2108–15.
[86] Wübbenhorst M, van Turnhout J, Klap GJ, Jansen JC, Quintel A, Hulliger J. Spontaneous polarization and orientational dynamics of polar rod-like molecules in host/guest materials. IEEE Trans Dielectr Electr Insul 2000;7:523–30.
[**87] Quintel A, Roth SW, Hulliger J, Wübbenhorst M. 3D-imaging and simulation of the polarization distribution in molecular crystals. Mol Cryst Liq Cryst 2000;338:243–56. Presents measurements of the spatial polarisation distribution in inhomogeneously polar molecular crystals by scanning pyroelectric microscopy (SPEM) and simulations by a Markov process. Using a tomographic method based on layerwise thinning of crystals 3D imaging of the polarization ditribution is achieved. Applied to perhydro- triphenylene (PHTP) co-crystallised with 1-(4-nitrophenyl)piperazine (NPP) two conical macro-domains of opposite and nearly constant polarisation were found which is in good agreement with a homogeneous Markov chain model driving dipolar molecules into a parallel state within channels of PHTP.
[**88] Gervais C, Wüst T, Behrnd NR, Wübbenhorst M, Hulliger J. Prediction of growth-induced polarity in centrosymmetric molecular crystals using force field methods. Chem Mater 2005;17:85–94. A three-step procedure is proposed to investigate growth-induced polarity arising in centrosymmetric crystals of dipolar molecules. It is based on (i) calculation of molecular interaction energies by force field methods, (ii) determination of the morphology, and (iii) use of the energies in a Markov-type growth mechanism on faces (hkl). Applied to trans-4-chloro-4′-nitrostilbene (CNS), the procedure showed that CNS crystals, although globally centric, are composed of sectors exhibiting different polar properties. The sectors related to the +b and −b directions show opposite polarity and are mainly responsible for observed second-harmonic generation and pyroelectric effects observed.
[**89] Behrnd NR, Wübbenhorst M, Hulliger J. Scanning pyroelectric microscopy revealing the spatial polarity distribution in topologically centric crystals of trans-4-chloro-4′-nitrostilbene. Phys Chem Chem Phys 2006;8:4132–7. Scanning pyroelectric microscopy is applied to investigate grown-in polarity in trans-4-chloro-4′-nitrostilbene (CNS) single crystals. Demonstrates a bipolar grown-in state of polarity for sector involving the twofold axis-*b*. These measurements agree with theoretical force field and stochastic calculations, predicting a bipolar state and a nearly identical extent of polarity for two different sectors.
[90] Cox SD, Gier TE, Stucky GD. Second harmonic generation by the self-aggregation of organic guests in molecular sieve hosts. Chem Mater 1990;2:609–19.
[91] Caro J, Finger G, Kornatowski J, Richter-Mendau J, Werner L, Zibrovious B. Aligned molecular sieve crystals. Adv Mater 1992;4:273–6.
[92] Hulliger J, Quintel A, Wübbenhorst M, Lanngley PJ, Roth SW, Rechsteiner P. Theory and pyroelectric characterization of polar inclusion compounds of perhydrotriphenylene. Opt Mater 1998;9:259–64.
[93] Sessler GM, West JE, Gerhard-Multhaupt R, von Seggern H. Nondestructive laser method for measuring charge profiles in irradiated polymer films. IEEE Trans Nucl Sci 1982;29:1644–9.
[94] Sessler GM, West JE, Gerhard G. High-resolution laser-pulse method for measuring charge distributions in dielectrics. Phys Rev Lett 1982;48: 563–6.
[95] Gerhard-Multhaupt R. Electrets: dielectrics with quasi-permanent charge or polarization. IEEE Trans Electr Insul 1987;EI-22:531–40.
[96] Tanaka A, Maeda M, Takada T. Observation of charge behavior in organic photoconductor using pressure-wave propagation method. IEEE Trans Electr Insul 1991;27:440–4.
[97] Motyl E. Pressure methods of space charge measurement in dielectrics. J Electrost 1997;40:469–76.
[98] Alquie C, Dreyfus G, Lewiner J. Stress-wave probing of electric field distributions in dielectrics. Phys Rev Lett 1981;47:1483–7.
[99] Takada T, Maeno T, Kushibe H. An electric stress pulse technique for the measurement of charges in a plastic plate irradiated by an electron beam. IEEE Trans Electr Insul 1987;22:497–501.
[100] Tanaka Y, Kitajima H, Kodaka M, Takada T. Analysis and discussion on conduction current based on simultaneous measurement of TSC and space charge distribution. IEEE Trans Dielectr Electr Insul 1998;5: 952–6.
[101] Takata K, Kushida K, Torii K, Miki H. Strain imaging of lead–zirconate–titanate thin film by tunneling acoustic microscopy. Jpn J Appl Phys 1994;33:3193–6.
[102] Takata K. Strain-imaging observation of a $Pb(Zr,Ti)O_3$ thin film. J Vac Sci Technol B 1996;14:882–6.
[103] Kolosov O, Gruverman A, Hatano J, Takahashi K, Tokumoto H. Nanoscale visualization and control of ferroelectric domains by atomic force microscopy. Phys Rev Lett 1995;74:4309–12.
[104] Gruverman A, Kholkin AL, Kingon A, Tokumoto H. Asymmetric nanoscale switching in ferroelectric thin films by scanning force microscopy. Appl Phys Lett 2001;78:2751–3.
[105] Kalinin SV, Bonnell DA. Imaging mechanism of piezoresponse force microscopy of ferroelectric surfaces. Phys Rev B 2002;65:125408.
[106] Amorin H, Shvartsman VV, Bdikin IK, Costa MEV, Kholkin AL, Pertsev NA. Ferroelectric domains and twinning in high-quality $SrBi_2Ta_2O_9$ crystals. Appl Phys Lett 2006;88:062903.
[107] Shvartsman VV, Kholkin AL, Verdier C, Lupascu DC. Fatigue-induced evolution of domain structure in ferroelectric PZT ceramics studied by piezoresponse force microscopy. J Appl Phys 2005;98:094109.
[108] Kholkin AL, Shvartsman VV, Woitas M, Safari A. Local electromechanical properties and grain size effects in ferroelectric relaxors studied by scanning piezoelectric microscopy. Mat Res Soc Symp Proc 2003;748:343–8.
[109] Wu D, Kunishima I, Roberts S, Gruverman A. Spatial variations in local switching parameters of ferroelectric random access memory capacitors. Appl Phys Lett 2009;95:092901.
[110] Sharma P, Reece T, Wu D, Fridkin VM, Ducharme S, Gruverman A. Nanoscale domain patterns in ultrathin polymer ferroelectric films. J Phys Condens Matter 2009;48:485902.
[111] Gruverman A, Cross JS, Oates WS. Peculiar effect of mechanical stress on polarization stability in micrometer-scale ferroelectric capacitors. J Mater Sci 2006;41:107–16.

[112] Kalinin SV, Rodriguez BJ, Jesse S, Chu YH, Zhao T, Ramesh R, et al. Intrinsic single-domain switching in ferroelectric materials on a nearly ideal surface. PNAS 2007;104:20204–9.

[113] Kim Y, Kim W, Choi H, Hong S, Ko H, Lee H, et al. Nanoscale domain growth dynamics of ferroelectric poly(vinylidene fluoride-co-trifluoroethylene) thin films. Appl Phys Lett 2010;96:012908.

[114] Kholkin AL, Kalinin SV, Roelofs A, Gruverman A. Review of ferroelectric domain imaging by piezoresponse force microscopy. In: Kalinin S, Gruverman A, editors. Scanning probe microscopy: electrical and electromechanical phenomena at the nanoscale. Springer; 2006.

[115**] Kalinin SV, Rar A, Jesse S. A decade of piezoresponse force microscopy: progress, challenges, and opportunities. IEEE Trans Ultrason Ferroelectr Freq Control 2006;53:2226–52. Thorough review of the theory, experimental pitfalls and practical applications of PFM.

[116] Kalinin SV, Borisevich AY, Jesse S, Rodriguez BJ, Morozovska A, Eliseev E, et al. Spatial resolution, information limit, and contrast transfer in piezoresponce force microscopy. Microsc Microanal 2007;13:1594–5.

[117] Kalinin SV, Rodriguez BJ, Kim S-H, Hong S-K, Gruverman A, Eliseev EA. Imaging mechanism of piezoresponse force microscopy in capacitor structures. Appl Phys Lett 2008;92:152906.

[118**] Bonnell DA, Kalinin SV, Kholkin AL, Gruverman A. Piezoresponse force microscopy: a window into electromechanical behavior at the nanoscale. Mater Res Bull 2009;34:648–57. Recent review covering a wide range of applications and recent experimental results using PFM.

[119] Kalinin SV, Bonnell DA. Surface potential at surface–interface junctions in $SrTiO_3$ bicrystals. Phys Rev B 2000;62:10419–30.

[120] Matsushige K, Yamada H, Tanaka H, Horiuchi T, Chen XQ. Nanoscale control and detection of electric dipoles in organic molecules. Nanotechnology 1998;9:208–11.

[**121] Kimura K, Kobayashi K, Yamada H, Horichi T, Ishida K, Matsushige K. Orientation control of poly(vinylidenefluoride–trifluoroethylene) crystals and molecules using atomic force microscopy. Appl Phys Lett 2003;82:4050–2. An aligning technique for polymer crystals and molecular chains utilizing contact-mode atomic force microscopy (AFM) is presented and applied to lamellar crystals and molecular chains of poly(vinylidenefluoride–trifluoroethylene) thin films.

[**122] Gautreau O, Harnagea C, Gunawan L, Nechache R, Singh MP, Fournier P, et al. Piezoresponse force microscopy and magnetic force microscopy characterization of γ-Fe_2O_3–$BiFeO_3$ nanocomposite/$Bi_{3.25}La_{0.75}Ti_3O_{12}$ multiferroic bilayers. J Magn Magn Mater 2009;321:1799–802.

[**123] Rodriguez BJ, Jesse S, Kalinin SV, Kim J, Ducharme S, Fridkin VM, et al. Appl Phys Lett 2007;90:122904. The multiferroic behavior of epitaxialbi-layered heterostructures is studied using piezoresponse force microscopy, magnetic force microscopy and magnetometry. Demonstrates the presence and switching of magnetic and ferroelectric domains within the same area of the sample.

[124] Karapetian E, Kachanov M, Sevostianov I. The principle of correspondence between elastic and piezoelectric problems. Arch Appl Mech 2002;72:564–87.

[125] Luo Y, Szafraniak I, Nagarajan V, Wehrspohn RB, Steinhart M, Wendorff JH, et al. Ferroelectric lead zirconate titanate and barium titanate nanotubes. Integr Ferroelect 2003;59:1513–20.

[126] Lang SB. Piezoelectricity, pyroelectricity and ferroelectricity in biomaterials: speculation on their biological significance. IEEE Trans Dielectr Electr Insul 2000;7:466–73.

[*127] Hulliger J. Connective tissue polarity unraveled by a Markov-chain mechanism of collagen fibril segment self-assembly. Biophys J 2003;84:3501–7. Proposes an explanation occurrence of pyroelectricity in tissues of living organisms based on a Markov-chain mechanism taking place during collagen fibril self-assembly in extracytoplasmic channels. A difference in the fusion probabilities for fibril termini is assumed to drive the self-assembly into partial macroscopic polar order.

[**128] Shin J, Rodriguez BJ, Baddorf AP, Thundat T, Karapetian E, Kachanov M, et al. Simultaneous elastic and electromechanical imaging by scanning probe microscopy: theory and applications to ferroelectric and biological materials. J Vac Sci Technol B 2005;23:2102–8. An approach for combined imaging of elastic and electromechanical properties of materials is presented. Applicability of this technique for elastic and electromechanical imaging with nanoscale resolution in materials such as ferroelectrics and biological tissues is demonstrated.

[*129] Kalinin SV, Rodriguez BJ, Jesse S, Thundat T, Gruverman A. Electromechanical imaging of biological systems with sub-10 nm resolution. Appl Phys Lett 2005;87:053901. Electromechanical imaging of tooth dentin and enamel is demonstrated with sub-10 nm resolution using piezoresponse force microscopy. Determines the piezoelectric domain size and local protein fiber ordering in dentin. The shape of a single protein fibril in enamel is visualized in real space and local hysteresis loops are measured.

[**130] Rodriguez BJ, Kalinin SV, Shin J, Jesse S, Grichko V, Thundat T, et al. Electromechanical imaging of biomaterials by scanning probe microscopy. J Struct Biol 2006;153:151–9. Nanostructural imaging of a variety of protein-based materials, including tooth, antler, and cartilage, is demonstrated. Visualization of protein fibrils with sub-10 nm spatial resolution in a human tooth is achieved.

[**131] Kalinin SV, Rodriguez BJ, Shin J, Jesse S, Grichko V, Thundat T, et al. Bioelectromechanical imaging by scanning probe microscopy: Galvani's experiment at the nanoscale. Ultramicroscopy 2006;106:334–40. Piezoresponse force microscopy is used to measure the sub-Angstrom mechanical response of a biological system induced by an electric bias applied to a conductive SPM tip. Visualization of the spiral shape and orientation of protein fibrils with 5 nm spatial resolution in a human tooth and chitin molecular bundle orientation in a butterfly wing is demonstrated. In particular, the applicability of SPM-based techniques for the determination of molecular orientation is discussed.

[*132] Rodriguez BJ, Jesse S, Habelitz S, Proksch R, Kalinin SV. Intermittent contact mode piezoresponse force microscopy in a liquid environment. Nanotechnology 2009;20:195701. The feasibility of intermittent contact mode piezoresponse force microscopy based on simultaneous mechanical and electrical probe modulation is explored. It is shown that imaging at frequencies corresponding to the first contact resonance in liquid allows contrast consistent with the electromechanical signal to be obtained for model ferroelectric systems and piezoelectric tooth dentin.

[**133] Minary-Jolandan M, Yu MF. Nanoscale characterization of isolated individual type I collagen fibrils: polarization and piezoelectricity. Nanotechnology 2009;20:085706. Piezoresponse force microscopy is applied to directly study individual type I collagen fibrils. It is shown that single collagen fibrils behave predominantly as shear piezoelectric materials with a piezoelectric coefficient on the order of 1 pm V^{-1}, and have unipolar axial polarization throughout their entire length. The result substantiates the nanoscale origin of piezoelectricity in bone and tendons, and implies also the potential importance of the shear load-transfer mechanism, which has been the principle basis of the nanoscale mechanics model of collagen, in mechanoelectric transduction in bone.

[134] Pollock HM, Hammiche A. Micro-thermal analysis: techniques and applications. J Phys D Appl Phys 2001;34:R23–53.

[**135] Antoniow JS, Chirtoc M, Trannoy N, Raphael O, Petzl J. Scanning thermal microscopy based on a modified atomic force microscope combined with pyroelectric detection. J Phys IV France 2005;125:113–6. A novel approach in scanning thermal microscopy of layered samples is presented based on the use of a Wollaston wire as a local a.c. heat source at the front of a sample layer deposited on a pyroelectric (PE) sensor. The thermal probe and PE signals are be used to generate complementary thermal conductivity and thermal diffusivity maps of the sample.